Sensitivity of Rydberg microwave electrometry limited by laser frequency noise

Bowen Yang [1,2,3] Yuhan Yan,[1,2,4] Xuejie Li,[1,2,4] Haojie Zhao,[1,2,3] Ling Xiao,[1,2] Xiaolin Li [1,5]
Jianliao Deng,[1,2,*] and Huadong Cheng [1,2,3,†]

[1]*Key Laboratory of Quantum Optics and Center of Cold Atom Physics, Shanghai Institute of Optics and Fine Mechanics,
Chinese Academy of Sciences, Shanghai 201800, China*
[2]*Wangzhijiang Innovation Center for Laser, Aerospace Laser Technology and System Department,
Shanghai Institute of Optics and Fine Mechanics, Chinese Academy of Sciences, Shanghai 201800, China*
[3]*Center of Materials Science and Optoelectronics Engineering, University of Chinese Academy of Sciences, Beijing 100049, China*
[4]*Department of Physics and Electronic Science, East China Normal University, Shanghai 200062, China*
[5]*School of Physics, East China University of Science and Technology, Shanghai 200237, China*

Laser frequency or phase noise is a main factor that limits the sensitivity of Rydberg microwave (MW) electrometry. In this study, we proposed a theoretical approach to estimate the effect of laser frequency noise on the atomic coherence of Rydberg sensors based on an atomic superheterodyne receiver. The noisy lasers were characterized using a phase-diffusion model. In particular, explicit formulas were derived to evaluate the noise-limited sensitivity for a given laser linewidth. Furthermore, the effect of Doppler broadening on the sensitivity of the Rydberg sensor at different atomic temperatures was estimated. Our theoretical results provide guidance for the development of Rydberg MW sensors and the method discussed herein can be applied to many other quantum systems.

I. INTRODUCTION

The accurate and precise measurement of physical quantities, including time, magnetic field intensity, and gravitational force, is of immense significance in the advancement of physics. These efforts have led to remarkable progress in quantum systems, such as optical clocks [1,2], atomic magnetometers [3,4], and atomic gravimeters [5,6]. Utilizing the properties of Rydberg atoms with large dipole moments [7], a new atomic sensor was proposed for measuring the incident microwave (MW) electric field amplitude. The motivation for developing Rydberg MW sensors stems from the superior performance of Rydberg sensors compared to those of traditional antenna-based sensors [8], and their potential applications in radar [8] and modern communication [9–13]. In Rydberg sensors, MW measurement is achieved by measuring the perturbations of atomic energy levels induced by incident MWs, such as the Autler-Townes (AT) splitting in the electromagnetically induced transparency (EIT) spectrum for strong MWs [14–21], and oscillating optical readout in atomic superheterodyne receivers for weak MWs [8,22,23].

Although the sensitivity of MW electrometry based on atomic superheterodyne receivers has reached an unprecedented level [8], it is still far from the fundamental limit predicted in Refs. [24,25]. The major noise that limits the sensitivity comprises two types of noise: laser noise, including the intensity and frequency noise, and atomic noise,

including quantum projection and atomic transit noise [26]. Laser frequency or phase noise usually degrades the sensor performance via phase-noise-to-intensity-noise conversion, which has been widely studied in absorption spectroscopy [27–30]. The spectral properties of a transmitted noisy laser in an EIT medium have also been extensively studied [31–37]. In addition, the noise spectra induced by the laser frequency noise have been used as a spectroscopic tool to measure the AT splitting [38]. However, methods for estimating the effect of laser frequency noise on the performance of Rydberg MW electrometry are lacking.

In this study, we theoretically investigate the conversion of laser frequency noise to atomic coherence noise in an atomic superheterodyne receiver. We propose a theoretical model for estimating the noise-limited sensitivity induced by laser frequency fluctuations. We focus on the variation of the coherence of the atomic system driven by noisy lasers modeled as a phase-diffusion field, and we obtain the noise power spectral density of atomic coherence by solving its stochastic differential equations (SDEs). Our results are significant for noise analysis in Rydberg MW electrometry and can be extended to other quantum sensors.

II. THEORETICAL MODEL

A. Description of the model

We briefly describe the principle of Rydberg MW electrometry based on atomic superheterodyne receivers. A typical experimental schematic diagram and a corresponding energy-level diagram are shown in Figs. 1(a) and 1(b),
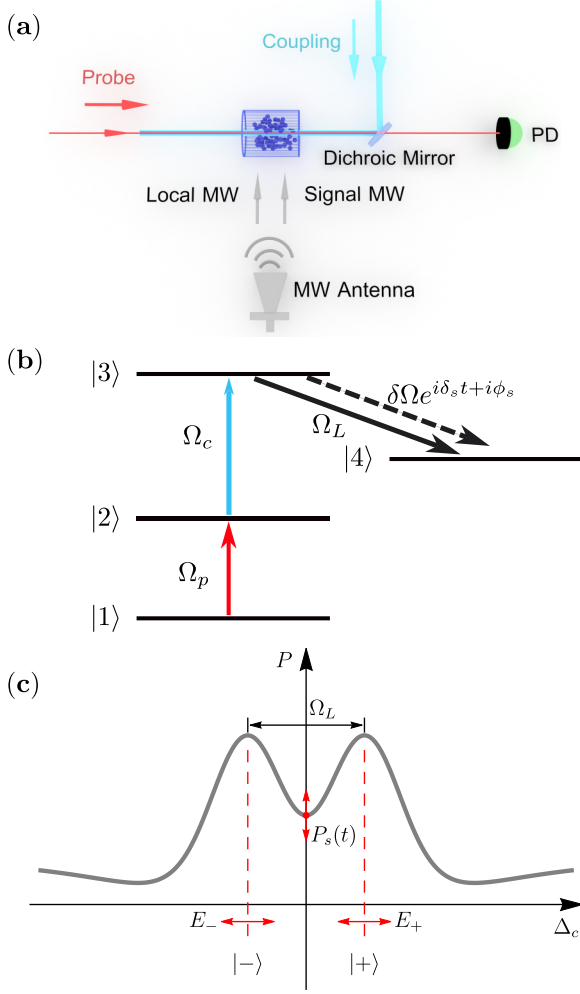
*jldeng@siom.ac.cn
†chenghd@siom.ac.cn

FIG. 1. (a) Typical experimental schematic for atomic super-heterodyne receiver. The probe and coupling laser beams counter-propagate through the cell and pump atoms to the Rydberg state. With the dressing of a strong local MW, the energy perturbation induced by a small signal MW is measured by recording the transmission signal of the probe laser using a photodetector (PD). (b) Atomic energy level scheme involved. Ω_p, Ω_c, and Ω_L are the Rabi frequencies of the probe, coupling, and local MW fields, respectively. The perturbed Rabi frequency of the weak signal MW is given by $\delta\Omega e^{i\delta_s t + \phi_s}$. The levels $|1\rangle$ and $|2\rangle$ denote ground and excited states, respectively, while the levels $|3\rangle$ and $|4\rangle$ are the two Rydberg states. (c) Example probe transmission signal P as a function of coupling detuning Δ_c in the presence of a strong local MW field. The strong resonant dressing of the local MW results in the appearance of AT splitting and two dressed states $|\pm\rangle = \frac{1}{\sqrt{2}}(|3\rangle \pm |4\rangle)$ energetically separated by $\hbar\Omega_L$. The small energy shifts $E_\pm = \pm\delta\Omega\cos(\delta_s t + \phi_s)$ induced by the weak signal MW for the dressed states leads to a dynamic change $P_s(t)$ in the resonant probe transmission, which then can be used to measure the amplitude and phase of the signal MW.

respectively. The probe, coupling, and local MW fields interact with atoms, generate the atomic coherence, and lead to the EIT-AT spectrum in the transmitted probe signal shown in Fig. 1(c). The two EIT peaks correspond to the two dressed states $|\pm\rangle$ (superposition of two Rydberg states, $|3\rangle$ and $|4\rangle$) induced by the strong local MW. Thus, the AT splitting of

the two EIT peaks is given by Ω_L for $\Omega_L \gg \Gamma_{\text{EIT}}$ (Γ_{EIT} is the linewidth of EIT), which is also the energy separation of two dressed states. The presence of weak signal MW $\delta\Omega$ perturbs two dressed states, leading to instantaneous energy shifts $E_\pm = \pm\delta\Omega\cos(\delta_s t + \phi_s)$ for two dressed states $|\pm\rangle$, where δ_s and ϕ_s are the frequency difference and the phase difference between local and signal MWs. This means both amplitude and phase information of the signal MW are encoded into the dynamic energy separation of two dressed states. As shown in Fig. 1(c), this variation is detected by measuring the amplitude of the transmitted probe light resonantly driving the atoms. For $\delta_s \ll \Gamma_{\text{EIT}}$, the dynamic change $P_s(t)$ in the resonant probe transmission induced by the weak signal MW field can be expressed as

$$P_s(t) = \left| \frac{dP_0}{d\Omega_L} \right| \delta\Omega \cos(\delta_s t + \phi_s), \tag{1}$$

where P_0 is the resonant probe transmission signal without the signal MW. According to Eq. (1), the oscillating optical readout can then be used to deduce the electric field amplitude of the incident signal MW. However, fluctuations in atomic coherence induced by the frequency noise of lasers limit the minimum measurable perturbation induced by the weak signal MW, providing noise-limited sensitivity for Rydberg MW electrometry.

B. Models for laser frequency fluctuations

The stochastic frequency or phase fluctuations of the probe and coupling lasers are described by the phase-diffusion model. Thus, the frequency noise is Gaussian δ-correlated, and the spectral shapes of the lasers are Lorentzian [30]. Assuming that the probe and coupling lasers are completely uncorrelated, the frequency fluctuations satisfy

$$\langle \delta\omega_{p,c}(t) \rangle = 0, \tag{2a}$$

$$\langle \delta\omega_{p,c}(t)\delta\omega_{p,c}(t+\tau) \rangle = \gamma_{p,c}\delta(\tau), \tag{2b}$$

$$\langle \delta\omega_p(t)\delta\omega_c(t+\tau) \rangle = 0, \tag{2c}$$

where the angular brackets $\langle\cdot\rangle$ denote the stochastic average; $\delta\omega_p(t)$ and $\delta\omega_c(t)$ denote the frequency fluctuations of the probe and coupling lasers, respectively; γ_p and γ_c are the linewidth (full width at half maximum) of the probe and coupling lasers, respectively; and $\delta(\tau)$ is the Dirac's delta function. Moreover, stochastic frequency fluctuations can be considered as formal derivatives of random-phase fluctuations. The corresponding stochastic-phase fluctuation $\phi_{p,c}(t)$ is modeled as a Wiener process (Brownian motion) with volatility $\sqrt{\gamma_{p,c}}$. Therefore, $\phi_{p,c}(t) = \sqrt{\gamma_{p,c}}W_{p,c}(t)$, where $W_{p,c}(t)$ is the standard Wiener process satisfying

$$\langle W_{p,c}(t) \rangle = 0, \tag{3a}$$

$$\langle W_{p,c}(t)W_{p,c}(t') \rangle = \min\{t, t'\}, \tag{3b}$$

$$\langle W_p(t)W_c(t') \rangle = 0. \tag{3c}$$

Here t and t' denote different moments in time, and min{} is the function returning the smallest value in a set of values.

C. Evolution equations of atomic coherence

The time evolution of the atomic density operator ρ is determined using the master equation [39]

$$\frac{d\rho}{dt} = -\frac{i}{\hbar}[H, \rho] + \mathcal{L}_\rho, \tag{4}$$

where H is the Hamiltonian for a single atom interacting with three external fields and $\mathcal{L}_\rho$ is the term that accounts for the relaxation processes. For theoretical simplicity, we restrict our discussion to the weak probe approximation. In this case, we have the following optical Bloch equation for atomic coherence:

$$\frac{d\rho_{12}}{dt} = -[\gamma_{12} + i\Delta_1 + i\delta\omega_p(t)]\rho_{12} + i\frac{\Omega_c}{2}\rho_{13} + i\frac{\Omega_p}{2}, \tag{5a}$$

$$\frac{d\rho_{13}}{dt} = -[\gamma_{13} + i\Delta_2 + i\delta\omega_p(t) + i\delta\omega_c(t)]\rho_{13}$$
$$+ i\frac{\Omega_c}{2}\rho_{12} + i\frac{\Omega_L}{2}\rho_{14}, \tag{5b}$$

$$\frac{d\rho_{14}}{dt} = -[\gamma_{14} + i\Delta_3 + i\delta\omega_p(t) + i\delta\omega_c(t)]\rho_{14} + i\frac{\Omega_L}{2}\rho_{13}, \tag{5c}$$

where γ_{12}, γ_{13}, and γ_{14} are the total the relaxation rates of the corresponding atomic coherence; $\Delta_1 = \Delta_p$, $\Delta_2 = \Delta_p + \Delta_c$, and $\Delta_3 = \Delta_p + \Delta_c - \Delta_L$ are the single-photon, two-photon, and three-photon detunings, respectively; $\delta\omega_p(t)$ and $\delta\omega_c(t)$ are the frequency fluctuations of the probe and coupling fields, respectively; and Δ_Z and Ω_Z ($Z \in \{p, c, L\}$) are the optical detuning and Rabi frequency of the corresponding field, respectively. The relaxation rate in a Rydberg atomic system is usually associated with the spontaneous decay rate, transit time broadening, atom-wall interactions, and atom-atom collisions [24]. In our theoretical model, we considered only the spontaneous decay rate and transit time broadening, because in hot atoms they are generally the main part for the experiment with small beam size, such as Ref. [11]. Then, the relaxation rates are given by

$$\gamma_{12} = \frac{\Gamma_2}{2} + \gamma_t, \quad \gamma_{13} = \gamma_{14} = \frac{\Gamma_r}{2} + \gamma_t, \tag{6}$$

where $\Gamma_2 = 2\pi \times 6.07\,\text{MHz}$ and $\Gamma_r = 2\pi \times 10\,\text{kHz}$ are the typical spontaneous decay rates of the excited and Rydberg states of ^{87}Rb atoms, respectively, and $\gamma_t = 2\pi \times 500\,\text{kHz}$ is the typical transit relaxation rate. Note that if other relaxation effects or atomic species are taken into account, we only need to modify the relaxation rate in the model. We retained these relaxation rates for all numerical simulations unless otherwise specified. In addition, in this study, we focused on the resonant condition for probe and local MW fields; thus, $\Delta_p = 0$ and $\Delta_L = 0$ in all calculations.

As the MW measurement relates to the amplitude of the transmitted light, we are interested in the variation of the imaginary part of atomic coherence. According to Eqs. (5a), (5b), and (5c), we can obtain similar evolution equations for the imaginary and real parts of the atomic coherence. Consider

the vector variable defined as

$$\begin{aligned} \boldsymbol{X} = \{ &\text{Re}(\rho_{12}), \text{Im}(\rho_{12}), \text{Re}(\rho_{13}), \\ &\text{Im}(\rho_{13}), \text{Re}(\rho_{14}), \text{Im}(\rho_{14}) \}^T, \end{aligned} \tag{7}$$

which satisfies the equation

$$\frac{d\boldsymbol{X}}{dt} = (\boldsymbol{F} + \delta\omega_p(t)\boldsymbol{B}_p + \delta\omega_c(t)\boldsymbol{B}_c)\boldsymbol{X} + \mathcal{C}, \tag{8}$$

where the definitions of the matrices $\boldsymbol{F}$, $\boldsymbol{B}_p$, $\boldsymbol{B}_c$, and the vector $\mathcal{C}$ are provided in Appendix A. The SDE of atomic coherence in the Stratonovich sense is given by

$$dX = (\boldsymbol{F}\boldsymbol{X} + \mathcal{C})dt + \sum_{i\in\{p,c\}} \sqrt{\gamma_i}\boldsymbol{B}_i\boldsymbol{X} \circ dW_i(t), \tag{9}$$

where $\circ$ denotes the Stratonovich integral, and $W_p(t)$ and $W_c(t)$ are the standard Wiener processes described in Sec. II B. A Stratonovich SDE can be converted to an equivalent SDE in the Itô sense by a simple transformation given by

$$dX = (\boldsymbol{F}'\boldsymbol{X} + \mathcal{C})dt + \sum_{i\in\{p,c\}} \sqrt{\gamma_i}\boldsymbol{B}_i\boldsymbol{X} dW_i(t), \tag{10}$$

where $\boldsymbol{F}' = \boldsymbol{F} + \gamma_p\boldsymbol{B}_p^2/2 + \gamma_c\boldsymbol{B}_c^2/2$. Appendix B provides the proof of Eq. (10). This transformation effectively adds laser decoherence rates to the relaxation rates of atomic coherence. Applying a stochastic average to both sides of Eq. (10), we obtain the evolution equation of $\langle \boldsymbol{X} \rangle$, which is given by

$$\frac{d\langle \boldsymbol{X} \rangle}{dt} = \boldsymbol{F}'\langle \boldsymbol{X} \rangle + \mathcal{C}. \tag{11}$$

This form is consistent with those report in Refs. [40,41]. For the steady-state condition (i.e., $t \to \infty$), we obtain the stationary stochastic average $\bar{\boldsymbol{X}} = \langle \boldsymbol{X}(\infty) \rangle$, which satisfies

$$\boldsymbol{F}'\bar{\boldsymbol{X}} + \mathcal{C} = 0. \tag{12}$$

D. Fluctuations of atomic coherence

We now consider the time evolution of the fluctuation in the atomic coherence, which is defined by $\Delta \boldsymbol{X}(t) = \boldsymbol{X}(t) - \bar{\boldsymbol{X}}$. Then, according to Eq. (11), the stochastic average of $\Delta \boldsymbol{X}$ follows a similar equation:

$$\frac{d\langle \Delta \boldsymbol{X} \rangle}{dt} = \boldsymbol{F}'\langle \Delta \boldsymbol{X} \rangle. \tag{13}$$

Furthermore, using the regression theorem [42,43], the stochastic average of the two-time correlation or covariance function of atomic coherence follows the same equation:

$$\frac{d\boldsymbol{C}(t + \tau, t)}{d\tau} = \boldsymbol{F}'\boldsymbol{C}(t + \tau, t), \tag{14}$$

where $\tau > 0$ and the matrix covariance function $\boldsymbol{C}(t, t')$ is defined as

$$\boldsymbol{C}(t, t') = \langle \Delta \boldsymbol{X}(t)\Delta \boldsymbol{X}^T(t') \rangle. \tag{15}$$

The covariance function can then be written as

$$\boldsymbol{C}(t, t') = \begin{cases} \exp[\boldsymbol{F}'(t - t')]\boldsymbol{P}(t'), & \text{if } t \geqslant t', \\ \boldsymbol{P}(t)\exp[\boldsymbol{F}'(t' - t)]^T, & \text{if } t < t', \end{cases} \tag{16}$$
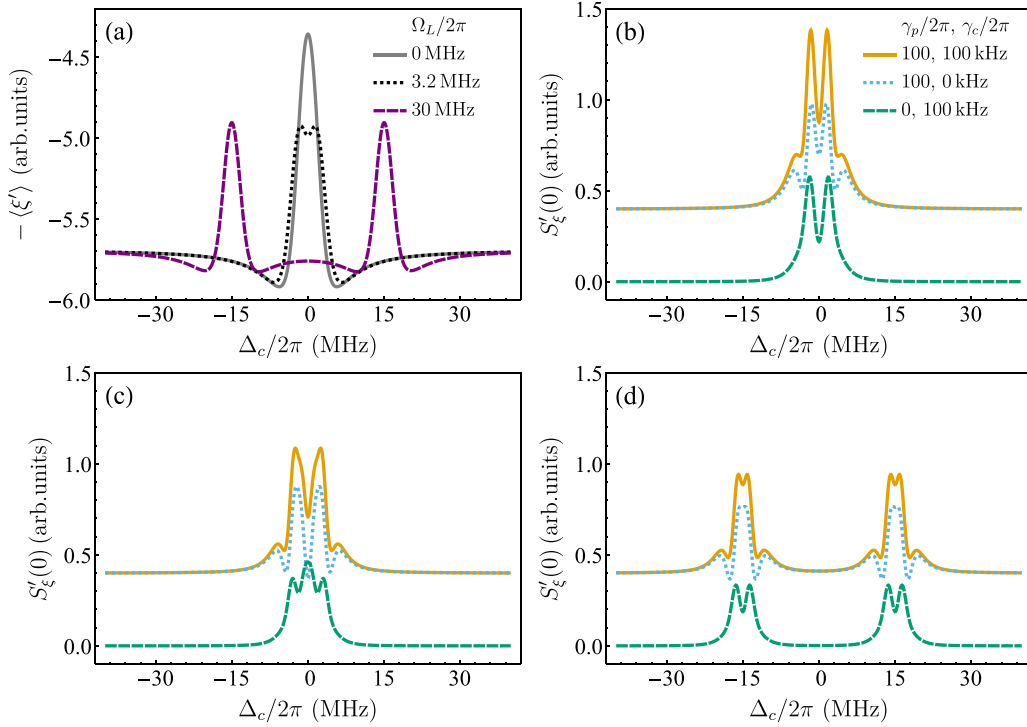
FIG. 2. (a) Negative of the Doppler-averaged atomic coherence as a function of Δ_c for different Rabi frequencies of local MW with $\Omega_c = 2\pi \times 3$ MHz and $\gamma_p = \gamma_c = 2\pi \times 100$ kHz. The Rabi frequency of local MW Ω_L varied from $\Omega_L/2\pi = 0$ MHz (solid gray line) to 3.2 MHz (dotted black line) to 30 MHz (dashed purple line). Panels (b), (c), and (d) correspond to the atomic coherence noise amplitude $S'_\xi(0)$ transferred from laser frequency noise versus Δ_c for $\Omega_L = 0$ MHz, $\Omega_L = 2\pi \times 3.2$ MHz, and $\Omega_L = 2\pi \times 30$ MHz, respectively. The noise spectra of atomic coherence contributed by the different values of laser frequency noise in panels (b), (c), and (d) are represented by solid yellow ($\gamma_p = \gamma_c = 2\pi \times 100$ kHz), dotted blue ($\gamma_p = 2\pi \times 100$ kHz and $\gamma_c = 0$ kHz), and dashed green ($\gamma_p = 0$ kHz and $\gamma_c = 2\pi \times 100$ kHz) lines, respectively.

where $\boldsymbol{P}(t) = \boldsymbol{C}(t, t)$. As we are interested in the stationary case, letting $\tau = t - t'$, the steady-state covariance or auto-correlation function $\boldsymbol{C}(\tau)$ becomes

$$\boldsymbol{C}(\tau) = \begin{cases} \exp{(\boldsymbol{F}'\tau)}\boldsymbol{P}(\infty), & \text{if } \tau \geqslant 0, \\ \boldsymbol{P}(\infty) \exp{(-\boldsymbol{F}'\tau)}^T, & \text{if } \tau < 0, \end{cases} \quad (17)$$

where $\boldsymbol{P}(\infty)$ denotes the steady-state covariance. Appendix C provides the derivation of $\boldsymbol{P}(\infty)$. According to the Wiener-Khinchin theorem, the Fourier transform of the autocorrelation function is the power spectral density (PSD). Thus, we have the following PSD matrix for the process $\Delta\boldsymbol{X}(t)$:

$$\boldsymbol{S}(\omega) = \frac{1}{2\pi} \int_{-\infty}^{\infty} d\tau \, \boldsymbol{C}(\tau) \exp{(-i\omega\tau)},$$
$$= \frac{1}{2\pi}[\boldsymbol{P}(\infty)(-\boldsymbol{F}' - i\omega\mathbf{I})^{-T} + (-\boldsymbol{F}' + i\omega\mathbf{I})^{-1}\boldsymbol{P}(\infty)], \quad (18)$$

where $\mathbf{I}$ denotes the identity matrix.

In addition, owing to the Doppler effect, the frequencies of the coupling and probe lasers seen by atoms with different velocities shift. Assuming that the noise of atomic coherence contributed by atoms with different velocity groups is completely uncorrelated, the PSD matrix with the Doppler average

is given by

$$\boldsymbol{S}'(\omega) = \frac{1}{\sqrt{\pi} v_p} \int_{-\infty}^{\infty} dv \, \boldsymbol{S}(\omega; \Delta'_p, \Delta'_c) e^{-v^2/v_p^2}, \quad (19)$$

where $v_p = \sqrt{2k_B T/m}$ denotes the most probable velocity of the atoms. In this integration, the probe and coupling laser detunings are modified to $\Delta'_p = \Delta_p - k_p v$ and $\Delta'_c = \Delta_c + k_c v$, where k_p and k_c are the wave vectors of the probe and coupling light, respectively. The Doppler effect cannot be ignored even for cold atoms because of the magnitude of the residual two-photon Doppler width being comparable to the natural linewidth of the Rydberg states (i.e., $|k_p - k_c|v_p/\Gamma_r \sim 6$ for $T = 30\,\mu$K). Unless otherwise specified, all numerical calculations were performed with $T = 300$ K.

III. RESULTS AND DISCUSSION

A. Noise power spectral density of atomic coherence

We focused on the imaginary part of the atomic coherence between $|1\rangle$ and $|2\rangle$, which is denoted by $\xi \equiv \text{Im}(\rho_{12})$, because it directly reflects the measured transmission signal. Furthermore, its mean value $\langle \xi' \rangle$ and noise PSD $S'_\xi(\omega)$ after the Doppler average can be directly obtained from Eqs. (12) and (19).

Figure 2(a) shows the numerical results for the EIT-AT spectrum with different local MW Rabi frequencies, and
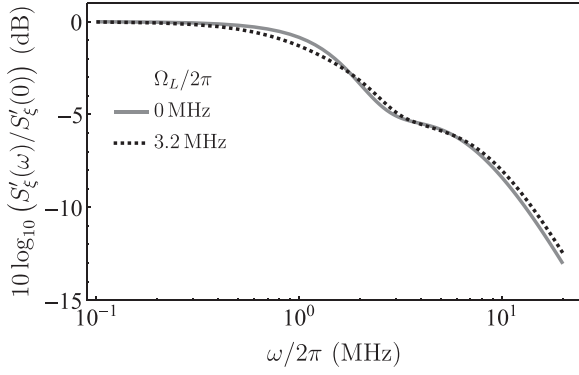
FIG. 3. The normalized noise PSD of atomic coherence $10 \log_{10}(S'_\xi(\omega)/S'_\xi(0))$ for $\Omega_L = 0$ MHz (solid gray line) and $\Omega_L = 2\pi \times 3.2$ MHz (dotted black line) with $\Omega_c = 2\pi \times 3$ MHz, $\Delta_c = 0$, and $\gamma_p = \gamma_c = 2\pi \times 100$ kHz.

Figs. 2(b)–2(d) show the corresponding noise amplitude $S'_\xi(0)$ of atomic coherence transferred from laser frequency noise as functions of coupling detuning Δ_c for different laser linewidths. It is apparent that two enhanced absorption dips can be observed near each EIT transmission peak shown in Fig. 2(a), which arises due to the wavelength mismatch between the coupling and probe lasers [44]. But we find that similar dips are also present in Figs. 2(b)–2(d), except for the noise spectra contributed from the coupling laser noise. This distinct behavior may be attributed to the fact that the frequency noise of the coupling laser does not contribute to the one-photon detuning Δ_1 and to the assumption of uncorrelated noise features for different velocity groups in Eq. (19). In addition, as shown in Fig. 2(d), a similar AT splitting appears in the noise spectra, which has been used for MW measurements [38].

We also analyzed the frequency distribution for the transferred atomic coherence noise. Although our theory assumes that the frequency noise of the laser is white noise, the response of the atomic system is finite, leading to a non-white-noise type of atomic coherence noise. Figure 3 shows two example noise PSDs of atomic coherence transferred from laser frequency noise. The noise PSD has a flat response at low frequencies, and the −3-dB bandwidth of the transferred atomic coherence noise is approximately 1.8 MHz. This reflects the response time of the atomic medium to some extent. The results also indicate that low-frequency noise may be characterized by a single noise value $S'_\xi(0)$.

B. Noise-limited sensitivity

We evaluated the noise-limited sensitivity of atomic superheterodyne receivers, which originates from the frequency noise of lasers, by considering the equivalent noise of the measured MW electric field amplitude. The small perturbation of atomic coherence $\delta\xi$ induced by the small incident signal MW δE satisfies

$$\delta\xi = \frac{d\xi}{d\Omega_L} \frac{\delta E \, d_R}{\hbar}, \qquad (20)$$

where d_R is the dipole moment between $|3\rangle$ and $|4\rangle$, and $\hbar$ is the reduced Planck's constant. Then, the equivalent one-sided
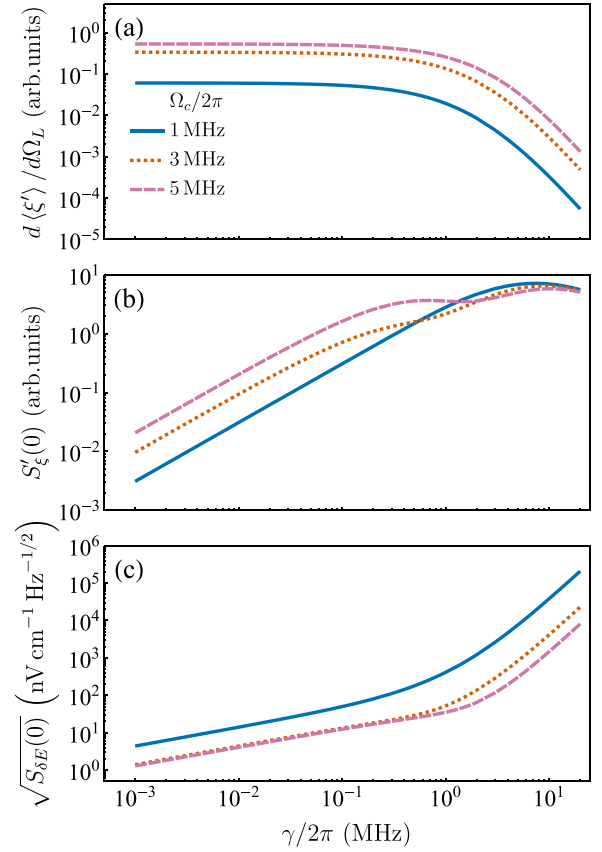

FIG. 4. Slope factor $d\langle\xi'\rangle/d\Omega_L$, noise PSD $S'_\xi(0)$, and noise-limited sensitivity $\sqrt{S_{\delta E}(0)}$ versus laser linewidth $\gamma = \gamma_p = \gamma_c$ for coupling Rabi frequencies $\Omega_c = 2\pi \times 1$ MHz (solid blue line), $\Omega_c = 2\pi \times 3$ MHz (dotted yellowish-brown line), and $\Omega_c = 2\pi \times 5$ MHz (dashed sky magenta line). (a) Slope factor. (b) Noise PSD. (c) Noise-limited sensitivity. For each coupling Rabi frequency Ω_c and laser linewidth γ, we chose an optimal Rabi frequency of the local MW Ω_L which maximized the slope factor.

noise PSD of δE is

$$S_{\delta E}(f) = 2\left(\frac{\hbar}{d_R} \frac{1}{(d\langle\xi'\rangle/d\Omega_L)}\right)^2 2\pi S'_\xi(2\pi f), \qquad (21)$$

where the factors 2 and 2π arise because $S'_\xi(2\pi f)$ is a two-sided noise PSD, and we focused on the PSD in the Fourier frequency f instead of the angular frequency ω. If we restrict our discussion to the low-frequency regime, the noise-limited sensitivity is given by $\sqrt{S_{\delta E}(0)}$. Furthermore, if we choose the Rydberg transition $51D_{5/2} \to 52P_{3/2}$ in ^{87}Rb for the π polarized field, the transition dipole moment with $m_j = 1/2$ (m_j is the magnetic quantum number) is given by $d_R = 1640.18 \, ea_0$ [45].

Figure 4 shows the slope factor $d\langle\xi'\rangle/d\Omega_L$, noise PSD $S'_\xi(0)$, and noise-limited sensitivity $\sqrt{S_{\delta E}(0)}$ as functions of the laser linewidth γ for different coupling Rabi frequencies. The reduction in slope factor and the increase in noise clearly deteriorate the sensitivity (lower value indicates better performance) as the laser linewidth increases. Compared to the fundamental sensitivity predicted in Refs. [24,25], our results indicate that the laser frequency noise could be the major factor limiting the sensitivity of Rydberg MW
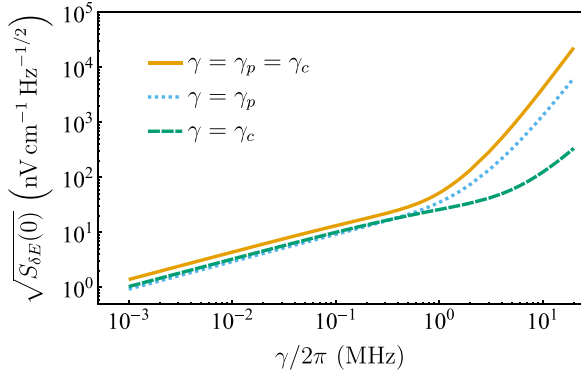
FIG. 5. Noise-limited sensitivity as a function of γ contributed by different laser linewidths with $\Omega_c = 2\pi \times 3\,\mathrm{MHz}$ and optimal Ω_L for each linewidth γ. The solid yellow, dotted blue, and dashed green lines correspond to $\gamma = \gamma_p = \gamma_c$, $\gamma = \gamma_p$, and $\gamma = \gamma_c$, respectively.

electrometry for large laser linewidths, which cannot be mitigated by an increase in the number of participating atoms. In addition, we find that the noise in the broad linewidth regime (i.e., $\gamma > 2\pi \times 10\,\mathrm{MHz}$) begins to decrease slightly with increasing laser linewidth, as shown in Fig. 4(b). This is similar to the behavior observed in the transmitted intensity noise in a resonant vapor cell [28] and may be due to the broadening effect induced by the increasing laser dephasing rates. Furthermore, we note that a strong coupling Rabi frequency is suitable for improving the sensitivity owing to an increase in the slope factor $d\langle\xi'\rangle/d\Omega_L$.

The limited sensitivities owing to the frequency noise of the coupling and probe lasers are shown in Fig. 5. In the small linewidth regime (i.e., $\gamma < 2\pi \times 800\,\mathrm{kHz}$), the noise-limited sensitivities contributed by the coupling and probe lasers are nearly equal, whereas in the broad linewidth regime (i.e., $\gamma > 2\pi \times 1\,\mathrm{MHz}$), the noise-limited sensitivity deteriorates rapidly with increasing linewidth and is dominated by the frequency fluctuations of the probe laser.

Furthermore, we analyzed the dependence of the slope factor, the noise PSD, and the noise-limited sensitivity on the atomic temperature to determine the role of the Doppler broadening effect in the noise conversion process, and the corresponding results are shown in Figs. 6(a)–6(c), respectively. We adjusted the transit relaxation γ_t with $\gamma_t = \gamma_0\sqrt{T/T_0}$, where $\gamma_0 = 2\pi \times 500\,\mathrm{kHz}$ is the transit relaxation rate at $T_0 = 300\,\mathrm{K}$, because of the decreased atomic velocities with the reduction in the atomic temperature. The slope factor $d\langle\xi'\rangle/d\Omega_L$ and the noise PSD $S'_\xi(0)$ clearly decrease with increasing atomic temperature. The noise-limited sensitivity varies slightly when the temperature is below 10 mK, whereas it worsens as the temperature increases from 10 mK to 80 K. Moreover, the improvement in the noise-limited sensitivity arises at a high temperature (i.e., $T > 80\,\mathrm{K}$). This can be attributed to the fact that the reduction in noise outweighs the effect of the decrease in the slope factor owing to the Doppler average effect.

Our theoretical analysis is based on the assumption of a Lorentzian shape of the laser spectrum. In a realistic case, the laser frequency is generally affected by flicker noise at low frequencies, which leads to a Gaussian line shape, and
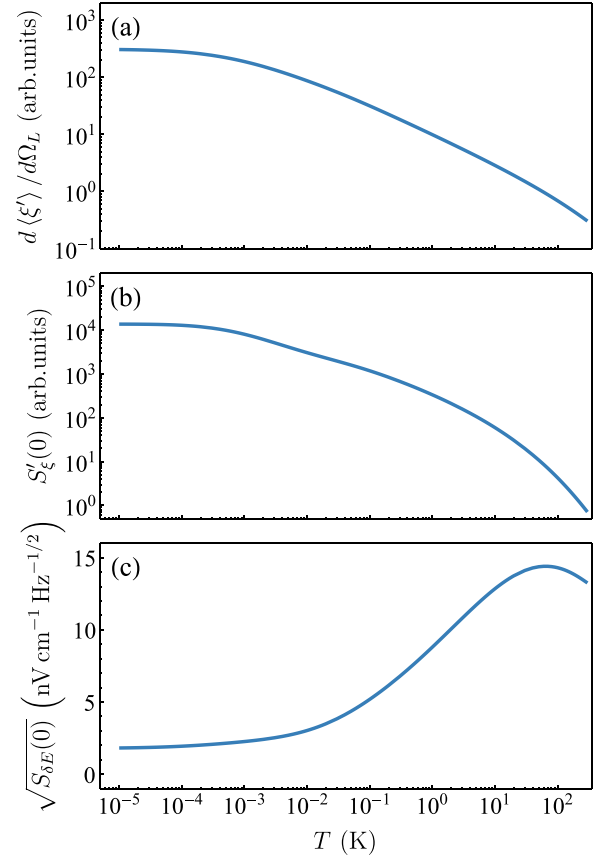

FIG. 6. Slope factor $d\langle\xi'\rangle/d\Omega_L$, noise PSD $S'_\xi(0)$, and noise-limited sensitivity $\sqrt{S_{\delta E}(0)}$ as a function of the atomic temperature T with $\Omega_c = 2\pi \times 3\,\mathrm{MHz}$, $\gamma_p = \gamma_c = 2\pi \times 100\,\mathrm{kHz}$, and optimal Ω_L maximizing $d\langle\xi'\rangle/d\Omega_L$ for each temperature. (a) Slope factor. (b) Noise PSD. (c) Noise-limited sensitivity.

white noise at high frequencies, which results in a Lorentzian line shape [46]. However, atomic superheterodyne receivers usually operate in the high-frequency regime to avoid $1/f$ noise. Thus, our scheme continues to reasonably estimate the influence of laser frequency noise on the sensitivity of MW electrometry. In addition, the transferred noise of atomic coherence, which stems from laser frequency fluctuations, might be underestimated in a practical atomic vapor cell, especially for an optically thick medium. This is because the incident laser noise in an atomic medium generates atomic coherence noise, which can reciprocally influence the laser and amplify noise generation.

IV. CONCLUSION

In conclusion, we have proposed a theoretical model to estimate the fundamental sensitivity of Rydberg MW electrometry limited by the frequency fluctuations of lasers. We established the correlation between the noise in atomic coherence and laser frequency by incorporating stochastic differential equations governing atomic coherence dynamics. We analyzed the noise-limited sensitivity of atomic superheterodyne receivers with different laser linewidths and their dependence on the atomic temperature. Our results provide guidance for determining the maximum frequency linewidth

of lasers to achieve future sensitivity limited by quantum projection noise. In addition, the proposed method can be directly extended to other quantum systems driven by noisy lasers, and hence, it is useful for applications such as atomic clocks and magnetometers.

ACKNOWLEDGMENTS

APPENDIX A: DEFINITION OF THE COEFFICIENTS IN EQ. (8)

The matrices $\boldsymbol{F}$, $\boldsymbol{B}_p$, and $\boldsymbol{B}_c$ and the vector $\boldsymbol{\mathcal{C}}$ are defined as

$$\boldsymbol{F} = \begin{pmatrix} -\gamma_{12} & \Delta_1 & 0 & -\Omega_c/2 & 0 & 0 \\ -\Delta_1 & -\gamma_{12} & \Omega_c/2 & 0 & 0 & 0 \\ 0 & -\Omega_c/2 & -\gamma_{13} & \Delta_2 & 0 & -\Omega_L/2 \\ \Omega_c/2 & 0 & -\Delta_2 & -\gamma_{13} & \Omega_L/2 & 0 \\ 0 & 0 & 0 & -\Omega_L/2 & -\gamma_{14} & \Delta_3 \\ 0 & 0 & \Omega_L/2 & 0 & -\Delta_3 & -\gamma_{14} \end{pmatrix},$$

$$\boldsymbol{B}_p = \begin{pmatrix} 0 & 1 & 0 & 0 & 0 & 0 \\ -1 & 0 & 0 & 0 & 0 & 0 \\ 0 & 0 & 0 & 1 & 0 & 0 \\ 0 & 0 & -1 & 0 & 0 & 0 \\ 0 & 0 & 0 & 0 & 0 & 1 \\ 0 & 0 & 0 & 0 & -1 & 0 \end{pmatrix},$$

$$\boldsymbol{B}_c = \begin{pmatrix} 0 & 0 & 0 & 0 & 0 & 0 \\ 0 & 0 & 0 & 0 & 0 & 0 \\ 0 & 0 & 0 & 1 & 0 & 0 \\ 0 & 0 & -1 & 0 & 0 & 0 \\ 0 & 0 & 0 & 0 & 0 & 1 \\ 0 & 0 & 0 & 0 & -1 & 0 \end{pmatrix},$$

$$\boldsymbol{\mathcal{C}} = (0 \quad \Omega_p/2 \quad 0 \quad 0 \quad 0 \quad 0)^T.$$

APPENDIX B: PROOF OF EQ. (10)

The difference between the Itô and Stratonovich senses is introduced in the definition of a stochastic integral. In most areas of physical science, where white noise is defined in terms of a δ-function autocorrelation, Stratonovich calculus is preferred [47]. However, we usually solve the SDEs in the Itô sense because the Stratonovich integral is not a martingale, which makes its theoretical analysis more difficult. A Stratonovich SDE can be converted into an equivalent Itô equation using the following algorithm [48].

Algorithm. A SDE in the Stratonovich sense,

$$dX = \boldsymbol{f}(X, t)dt + \boldsymbol{L}(X, t) \circ d\boldsymbol{W}(t) \tag{B1}$$

is equivalent to the following SDE in the Itô sense:

$$dX = \boldsymbol{f}'(X, t)dt + \boldsymbol{L}(X, t)d\boldsymbol{W}(t), \tag{B2}$$

where $\boldsymbol{f}(\boldsymbol{X}, t)$ is a vector-valued function, $\boldsymbol{L}(\boldsymbol{X}, t)$ is a matrix-valued function, $\boldsymbol{W}(t)$ is the vector Wiener process, and $\boldsymbol{f}'(\boldsymbol{X}, t)$ is given by

$$f_i'(\boldsymbol{X}, t) = f_i(\boldsymbol{X}, t) + \frac{1}{2}\sum_{j,l}\frac{\partial L_{ij}(\boldsymbol{X}, t)}{\partial X_l}L_{lj}(\boldsymbol{X}, t). \tag{B3}$$

In the case of Eq. (9), $\boldsymbol{f}(\boldsymbol{X}, t)$, $\boldsymbol{L}(\boldsymbol{X}, t)$, and $\boldsymbol{W}(t)$ can be expressed as

$$\boldsymbol{f}(\boldsymbol{X}, t) = \boldsymbol{F}\boldsymbol{X} + \boldsymbol{\mathcal{C}}, \tag{B4a}$$

$$\boldsymbol{L}(\boldsymbol{X}, t) = (\sqrt{\gamma_p}\boldsymbol{B}_p\boldsymbol{X} \quad \sqrt{\gamma_c}\boldsymbol{B}_c\boldsymbol{X}), \tag{B4b}$$

$$\boldsymbol{W}(t) = (W_p(t) \quad W_c(t))^T. \tag{B4c}$$

Then, according to Eq. (B3), we derive the following relationship:

$$\begin{aligned} f_i'(\boldsymbol{X}, t) &= \sum_j F_{ij}X_j + \mathcal{C}_i + \frac{1}{2}\sum_l \left(\frac{\partial L_{i1}(\boldsymbol{X}, t)}{\partial X_l}L_{l1}(\boldsymbol{X}, t)\right. \\ &\quad \left.+ \frac{\partial L_{i2}(\boldsymbol{X}, t)}{\partial x_l}L_{l2}(\boldsymbol{X}, t)\right) \\ &= \sum_j F_{ij}X_j + \mathcal{C}_i + \frac{1}{2}\sum_{l,j}(\gamma_p B_{p_{il}}B_{p_{lj}}X_j \\ &\quad + \gamma_c B_{c_{il}}B_{c_{lj}}X_j) \\ &= \sum_j F_{ij}X_j + \mathcal{C}_i + \frac{1}{2}\sum_j \left(\gamma_p(\boldsymbol{B}_p^2)_{ij}X_j\right. \\ &\quad \left.+ \gamma_c(\boldsymbol{B}_c^2)_{ij}X_j\right). \end{aligned} \tag{B5}$$

Thus, expressing Eq. (B5) in vector form, we obtain

$$\boldsymbol{f}'(X, t) = \left(\boldsymbol{F} + \gamma_p\boldsymbol{B}_p^2/2 + \gamma_c\boldsymbol{B}_c^2/2\right)X + \boldsymbol{\mathcal{C}}. \tag{B6}$$

Subsequently, Eq. (10) is proved.

APPENDIX C: DERIVATION OF $\boldsymbol{P}(\infty)$

According to Eq. (10), the SDE of $\Delta X(t)$ is given by

$$d\Delta X = \boldsymbol{F}'\Delta X dt + \sum_{i\in\{p,c\}}\sqrt{\gamma_i}\boldsymbol{B}_i(\Delta X + \bar{X})dW_i(t), \tag{C1}$$

Then the ordinary differential equation for the matrix second moment $\boldsymbol{P}(t)$ is given by [49]

$$\frac{d\boldsymbol{P}}{dt} = \boldsymbol{F}'\boldsymbol{P} + \boldsymbol{P}\boldsymbol{F}'^T + \sum_{i\in\{p,c\}}\gamma_i\boldsymbol{B}_i\boldsymbol{P}\boldsymbol{B}_i^T + \boldsymbol{\mathcal{B}}(t), \tag{C2}$$

where

$$\boldsymbol{\mathcal{B}}(t) = \sum_{i\in\{p,c\}}\gamma_i\boldsymbol{B}_i(\boldsymbol{m}(t)\bar{X}^T + \bar{X}\boldsymbol{m}^T(t) + \bar{X}\bar{X}^T)\boldsymbol{B}_i^T,$$

$$\boldsymbol{m}(t) = \langle\Delta X(t)\rangle. \tag{C3}$$

Thus, for the steady-state case, the stationary covariance $\boldsymbol{P}(\infty)$ obeys the equation

$$\boldsymbol{F}'\boldsymbol{P}(\infty) + \boldsymbol{P}(\infty)\boldsymbol{F}'^T + \sum_{i\in\{p,c\}}\gamma_i\boldsymbol{B}_i(\boldsymbol{P}(\infty) + \bar{X}\bar{X}^T)\boldsymbol{B}_i^T = 0. \tag{C4}$$

The numerical solution of Eq. (C4) yields a solution of $\boldsymbol{P}(\infty)$.

[1] E. Oelker, R. B. Hutson, C. J. Kennedy, L. Sonderhouse, T. Bothwell, A. Goban, D. Kedar, C. Sanner, J. M. Robinson, G. E. Marti, D. G. Matei, T. Legero, M. Giunta, R. Holzwarth, F. Riehle, U. Sterr, and J. Ye, Demonstration of 4.8×10^{-17} stability at 1 s for two independent optical clocks, Nat. Photon. **13**, 714 (2019).

[2] P. Fang, H. Sun, Y. Wang, Y. Xu, and Q. Chen, Transfer of laser frequency from 729 nm to 1.5 μm with precision at the level of 10^{-20}, Chin. Opt. Lett. **20**, 081403 (2022).

[3] L. Rondin, J.-P. Tetienne, T. Hingant, J.-F. Roch, P. Maletinsky, and V. Jacques, Magnetometry with nitrogen-vacancy defects in diamond, Rep. Prog. Phys. **77**, 056503 (2014).

[4] S. Zhang, J. Lu, Y. Zhou, F. Lu, K. Yin, D. Zhan, Y. Zhai, and M. Ye, Zero field optically pumped magnetometer with independent dual-mode operation, Chin. Opt. Lett. **20**, 081202 (2022).

[5] V. Menoret, P. Vermeulen, N. Le Moigne, S. Bonvalot, P. Bouyer, A. Landragin, and B. Desruelle, Gravity measurements below 10^{-9} g with a transportable absolute quantum gravimeter, Sci. Rep. **8**, 12300 (2018).

[6] Z.-K. Hu, B.-L. Sun, X.-C. Duan, M.-K. Zhou, L.-L. Chen, S. Zhan, Q.-Z. Zhang, and J. Luo, Demonstration of an ultrahigh-sensitivity atom-interferometry absolute gravimeter, Phys. Rev. A **88**, 043610 (2013).

[7] C. S. Adams, J. D. Pritchard, and J. P. Shaffer, Rydberg atom quantum technologies, J. Phys. B: At., Mol. Opt. Phys. **53**, 012002 (2019).

[8] M. Jing, Y. Hu, J. Ma, H. Zhang, L. Zhang, L. Xiao, and S. Jia, Atomic superheterodyne receiver based on microwave-dressed Rydberg spectroscopy, Nat. Phys. **16**, 911 (2020).

[9] K. C. Cox, D. H. Meyer, F. K. Fatemi, and P. D. Kunz, Quantum-limited atomic receiver in the electrically small regime, Phys. Rev. Lett. **121**, 110502 (2018).

[10] C. Holloway, M. Simons, A. H. Haddab, J. A. Gordon, D. A. Anderson, G. Raithel, and S. Voran, A multiple-band Rydberg atom-based receiver: AM/FM stereo reception, IEEE Antennas Propag. Mag. **63**, 63 (2021).

[11] D. H. Meyer, K. C. Cox, F. K. Fatemi, and P. D. Kunz, Digital communication with Rydberg atoms and amplitude-modulated microwave fields, Appl. Phys. Lett. **112**, 211108 (2018).

[12] D. H. Meyer, P. D. Kunz, and K. C. Cox, Waveguide-coupled Rydberg spectrum analyzer from 0 to 20 GHz, Phys. Rev. Appl. **15**, 014053 (2021).

[13] K. Yang, Z. Sun, R. Mao, Y. Lin, Y. Liu, Q. An, and Y. Fu, Wide-band Rydberg atom-based receiver for amplitude modulation radio frequency communication, Chin. Opt. Lett. **20**, 081203 (2022).

[14] D. A. Anderson, R. E. Sapiro, and G. Raithel, A self-calibrated SI-traceable Rydberg atom-based radio frequency electric field probe and measurement instrument, IEEE Trans. Antennas Propag. **69**, 5931 (2021).

[15] C. L. Holloway, J. A. Gordon, S. Jefferts, A. Schwarzkopf, D. A. Anderson, S. A. Miller, N. Thaicharoen, and G. Raithel, Broadband Rydberg atom-based electric-field probe for SI-traceable, self-calibrated measurements, IEEE Trans. Antennas Propag. **62**, 6169 (2014).

[16] K.-Y. Liao, H.-T. Tu, S.-Z. Yang, C.-J. Chen, X.-H. Liu, J. Liang, X.-D. Zhang, H. Yan, and S.-L. Zhu, Microwave electrometry via electromagnetically induced absorption in cold Rydberg atoms, Phys. Rev. A **101**, 053432 (2020).

[17] J. A. Sedlacek, A. Schwettmann, H. Kübler, R. Löw, T. Pfau, and J. P. Shaffer, Microwave electrometry with Rydberg atoms in a vapour cell using bright atomic resonances, Nat. Phys. **8**, 819 (2012).

[18] J. A. Sedlacek, A. Schwettmann, H. Kubler, and J. P. Shaffer, Atom-based vector microwave electrometry using rubidium Rydberg atoms in a vapor cell, Phys. Rev. Lett. **111**, 063001 (2013).

[19] M. T. Simons, A. B. Artusio-Glimpse, C. L. Holloway, E. Imhof, S. R. Jefferts, R. Wyllie, B. C. Sawyer, and T. G. Walker, Continuous radio-frequency electric-field detection through adjacent Rydberg resonance tuning, Phys. Rev. A **104**, 032824 (2021).

[20] M. T. Simons, J. A. Gordon, and C. L. Holloway, Simultaneous use of Cs and Rb Rydberg atoms for dipole moment assessment and RF electric field measurements via electromagnetically induced transparency, J. Appl. Phys. **120**, 123103 (2016).

[21] S. Zhao, Z. Yin, X. Song, Z. Jia, L. Wang, B. Chen, Q. Zeng, and Y. Peng, Enhanced microwave metrology using an optical grating in Rydberg atoms, Appl. Opt. **62**, 3747 (2023).

[22] Y. Cui, F.-D. Jia, J.-H. Hao, Y.-H. Wang, F. Zhou, X.-B. Liu, Y. H. Yu, J. Mei, J.-H. Bai, Y.-Y. Bao, D. Hu, Y. Wang, Y. Liu, J. Zhang, F. Xie, and Z.-P. Zhong, Extending bandwidth sensitivity of Rydberg-atom-based microwave electrometry using an auxiliary microwave field, Phys. Rev. A **107**, 043102 (2023).

[23] X.-H. Liu, K.-Y. Liao, Z.-X. Zhang, H.-T. Tu, W. Bian, Z.-Q. Li, S.-Y. Zheng, H.-H. Li, W. Huang, H. Yan, and S.-L. Zhu, Continuous-frequency microwave heterodyne detection in an atomic vapor cell, Phys. Rev. Appl. **18**, 054003 (2022).

[24] H. Fan, S. Kumar, J. Sedlacek, H. Kübler, S. Karimkashi, and J. P. Shaffer, Atom based RF electric field sensing, J. Phys. B: At., Mol. Opt. Phys. **48**, 202001 (2015).

[25] D. H. Meyer, C. O'Brien, D. P. Fahey, K. C. Cox, and P. D. Kunz, Optimal atomic quantum sensing using electromagnetically-induced-transparency readout, Phys. Rev. A **104**, 043103 (2021).

[26] Z. Wang, M. Jing, P. Zhang, S. Yuan, H. Zhang, L. Zhang, L. Xiao, and S. Jia, Noise analysis of the atomic superheterodyne receiver based on flat-top laser beams, Opt. Express **31**, 19909 (2023).

[27] J. C. Camparo, Conversion of laser phase noise to amplitude noise in an optically thick vapor, J. Opt. Soc. Am. B **15**, 1177 (1998).

[28] J. C. Camparo and J. G. Coffer, Conversion of laser phase noise to amplitude noise in a resonant atomic vapor: The role of laser linewidth, Phys. Rev. A **59**, 728 (1999).

[29] J. G. Coffer, M. Anderson, and J. C. Camparo, Collisional dephasing and the reduction of laser phase-noise to amplitude-noise conversion in a resonant atomic vapor, Phys. Rev. A **65**, 033807 (2002).

[30] R. Walser and P. Zoller, Laser-noise-induced polarization fluctuations as a spectroscopic tool, Phys. Rev. A **49**, 5067 (1994).

[31] M. Fleischhauer, Correlation of high-frequency phase fluctuations in electromagnetically induced transparency, Phys. Rev. Lett. **72**, 989 (1994).

[32] M. T. L. Hsu, G. Hetet, O. Glockl, J. J. Longdell, B. C. Buchler, H. A. Bachor, and P. K. Lam, Quantum study of information delay in electromagnetically induced transparency, Phys. Rev. Lett. **97**, 183601 (2006).

[33] A. F. Huss, R. Lammegger, C. Neureiter, E. A. Korsunsky, and L. Windholz, Phase correlation of laser waves with arbitrary frequency spacing, Phys. Rev. Lett. **93**, 223601 (2004).

[34] E. E. Mikhailov, V. A. Sautenkov, Y. V. Rostovtsev, A. Zhang, M. S. Zubairy, M. O. Scully, and G. R. Welch, Spectral narrowing via quantum coherence, Phys. Rev. A **74**, 013807 (2006).

[35] V. A. Sautenkov, Y. V. Rostovtsev, and M. O. Scully, Switching between photon-photon correlations and Raman anticorrelations in a coherently prepared Rb vapor, Phys. Rev. A **72**, 065801 (2005).

[36] Y. Xiao, T. Wang, M. Baryakhtar, M. Van Camp, M. Crescimanno, M. Hohensee, L. Jiang, D. F. Phillips, M. D. Lukin, S. F. Yelin, and R. L. Walsworth, Electromagnetically induced transparency with noisy lasers, Phys. Rev. A **80**, 041805(R) (2009).

[37] D. Yu and J. Chen, Optical clock with millihertz linewidth based on a phase-matching effect, Phys. Rev. Lett. **98**, 050801 (2007).

[38] J. He, Q. Liu, Z. Yang, Q. Niu, X. Ban, and J. Wang, Noise spectroscopy with a Rydberg ensemble in a hot atomic vapor cell, Phys. Rev. A **104**, 063120 (2021).

[39] M. Fleischhauer, A. Imamoglu, and J. P. Marangos, Electromagnetically induced transparency: Optics in coherent media, Rev. Mod. Phys. **77**, 633 (2005).

[40] S. N. Dixit, P. Zoller, and P. Lambropoulos, Non-Lorentzian laser line shapes and the reversed peak asymmetry in double optical resonance, Phys. Rev. A **21**, 1289 (1980).

[41] K. Wodkiewicz, Stochastic incoherences of optical Bloch equations, Phys. Rev. A **19**, 1686 (1979).

[42] C. Gardiner, in *Stochastic Methods: A Handbook for the Natural and Social Sciences*, 4th ed. (Springer, Berlin, 2010), p. 108.

[43] M. Lax, Quantum noise. XI. Multitime correspondence between quantum and classical stochastic processes, Phys. Rev. **172**, 350 (1968).

[44] A. K. Mohapatra, T. R. Jackson, and C. S. Adams, Coherent optical detection of highly excited Rydberg states using electromagnetically induced transparency, Phys. Rev. Lett. **98**, 113003 (2007).

[45] N. Šibalić, J. D. Pritchard, C. S. Adams, and K. J. Weatherill, ARC: An open-source library for calculating properties of alkali Rydberg atoms, Comput. Phys. Commun. **220**, 319 (2017).

[46] G. Di Domenico, S. Schilt, and P. Thomann, Simple approach to the relation between laser frequency noise and laser line shape, Appl. Opt. **49**, 4801 (2010).

[47] W. Moon and J. S. Wettlaufer, On the interpretation of Stratonovich calculus, New J. Phys. **16**, 055017 (2014).

[48] S. Sarkkä and A. Solin, in *Applied Stochastic Differential Equations* (Cambridge University Press, Cambridge, England, 2019), p. 55.

[49] J. C. Jimenez, Simplified formulas for the mean and variance of linear stochastic differential equations, Appl. Math. Lett. **49**, 12 (2015).